J. Innovative Eng. Nat. Sci., vol. 6, no. 2, pp. 563-583, 2026.
http://doi.org/10.61112/jiens.1882611

Original Paper

Journal of Innovative Engineering and Natural Science
(Yenilikçi Mühendislik ve Doğa Bilimleri Dergisi)
https://dergipark.org.tr/en/pub/jiens

An open-source target spectrum based artificial ground motion generation software

Bilal Tayfur [a,*]

[a]*Civil Engineering Department, Faculty of Engineering, Hacettepe University, 06800, Ankara, Türkiye.*

ARTICLE INFO

Article history:
Received February 5, 2026
Received in revised form May 30, 2026
Accepted June 30, 2026

Available online

Keywords:
Artificial ground motion
TBEC
Open source
Optimization

ABSTRACT

In certain special cases, it may be necessary to generate artificial ground motion records for seismic analysis of structures in time domain. This paper presents an open-source Python software that generates artificial ground motions in accordance with the target response spectrum generated per regulations including Turkish Building Earthquake Code 2018 (TBEC 2018). The software divides the steps of this process into modules, separated by strict boundaries. Firstly, the user determines the regulation and related parameters that will generate the target spectrum. Then the algorithm generates the white noise which is the basis of the ground motion. It is desired that the ground motion to be generated should have the characteristics of a real ground motion as much as possible. For this reason, software applies filtering and enveloping functions to the white noise to create vibration data with complex signal characteristics similar to real ground motions. Subsequently, the response spectrum of the ground motion record is aimed to converge to the target spectrum. To achieve this, the algorithm applies iterative spectral matching to the raw ground motion. At this point, the average error and maximum error values are taken as evaluation criteria.

I. INTRODUCTION

Probabilistic seismic hazard analysis underlies modern earthquake engineering practice. It supplies site-specific intensity measures such as 5%-damped response spectral accelerations and uniform hazard spectra for structural design and evaluation [1]. In complex tectonic environments where shallow crustal, subduction interface, and in-slab sources contribute simultaneously, building analysis-consistent input motions from real ground motion databases is difficult. Source type, path effects, and local site conditions all influence ground motions in ways that are not uniformly represented by global or imported datasets [2-7]. One limitation is tectonic mismatch, where records from one tectonic setting are applied to regions with different source mechanics or path properties. Seismic hazard assessments in Cascadia, for example, historically relied on empirical relations developed for California for shallow crustal events, while subduction events were modelled using relations from other regions [6,7]. When databases are not drawn from the same source regime, path attenuation structure, and stress-drop characteristics, direct record use or model transfer can introduce systematic bias [4,8].

In most cases, existing databases are adequate for a code-compliant and reliable seismic assessment [9,10]. However, real ground motion databases also tend to be sparse where site-specific analysis needs them most: large magnitudes, short distances, and near-fault conditions. Near-fault recordings of moderate-to-large events are rare, which limits prediction for the scenarios that typically govern structural damage [11-13]. The gap is widest in low-to-moderate seismicity regions, where return periods are long enough that few observations exist in either time or space [14]. Empirical hazard assessments often homogenize recordings under an ergodic assumption: that the median and variability for a given scenario are the same across all locations used to fit the model [3,15]. The

*Corresponding author. Tel.: +90 312 297 7328; e-mail: btayfur@hacettepe.edu.tr

assumption breaks down in tectonic settings shaped by specific fault rupture processes and local geology. Effects such as basin orientation and directional waveguiding are spatially systematic, and they are smeared when records are mixed ergodically [16-18]. Site characterization compounds this: subsurface data are often inadequate, and site factors do not transfer cleanly between tectonic regions [19-21]. Record selection is hardest when multiple tectonic sources contribute, and when features that matter at collapse-level limit states, such as duration and near-source pulses, are not captured by spectral shape alone [2,22-24].

Artificial (synthetic) ground motion time histories have become standard practice for these reasons. They are used when recorded motions are insufficient for controlling scenarios such as large-magnitude events at short distances or near-fault conditions, because empirical strong-motion datasets are thin in those regimes [13,14,25,26]. The literature divides artificial ground motion (AGM) generation into two broad categories [27]: methods that approximate the target spectrum by reshaping the frequency content of an existing motion, and methods that use white noise driven through specific processes to mimic real ground motions. The synthesis approaches in use span stochastic simulation combining a parametric amplitude spectrum with random phase and magnitude–distance-dependent duration models [25,28], site-based stochastic models that fit parameterized nonstationary processes [29-31], physics-based 3D wave propagation simulations for basin effects and spatial variability [32,33], hybrid broadband methods coupling deterministic low-frequency and stochastic high-frequency components [34-36], and, more recently, machine-learning synthesis using neural operators and diffusion models [37-38]. In addition, data-driven and machine learning algorithms are frequently used in the field of structural engineering [39-41].

Despite these methodological advances, open-source implementations remain limited. EXSIM, an open-source stochastic finite-fault simulation algorithm, has been applied for seismic zonation with site-specific soil effects [42], and SPEED, a 3D physics-based code, has been validated against near-source broadband recordings [43,44]. Regulation-adaptive tools that target international code compatibility with spectrum-compatible artificial earthquake generation are not well integrated into widely available open-source platforms [45,46]. Existing tools also face practical gaps: fragmentation of published methods limits reproducibility [5], incomplete accommodation of tectonic mixtures makes regional transferability challenging [6,8], and generalizing nonergodic behavior into accessible workflows is difficult [3,16]. Spectrum compatibility alone is also insufficient: response spectra do not capture properties relevant to nonlinear site response, nor non-spectral features such as duration and pulses that govern structural fragility [47-49].

This study presents an open-source Python software for generating artificial ground motions compatible with the design spectra of the Turkish Building Earthquake Code (TBEC) [50]. The workflow includes stochastic noise generation, Kanai–Tajimi/Clough–Penzien filtering, envelope shaping, and iterative spectral matching. Each step follows established procedures. The contribution here is to arrange them in a transparent framework: an object-oriented architecture with interchangeable components, namely the target spectrum generator, initial motion generator, filtering routine, envelope function, PGA estimator, and spectral matching kernel. All share a consistent interface, and any can be replaced for specific requirements. Users can swap or extend a single stage without touching the surrounding pipeline. An optional variant tunes seven hyperparameters simultaneously against the spectral-matching objective using a Teaching–Learning-Based Optimization (TLBO) algorithm; it converges more tightly but takes substantially more computation. Four alternative PGA estimation routines are also included. A parametric robustness analysis under varying TBEC parameters held average matching errors below 10%; the TLBO variant reduced them below 5% under stricter settings.

II. THEORETICAL BACKGROUND

The developed artificial ground motion generation software [51] rests on a set of theoretical foundations covered in this section. The artificial ground motion generation process has four main stages: building the target design spectrum, generating the white noise signal, obtaining the raw ground motion through filtering and envelope application, and matching the ground motion to the target spectrum. Several utility modules support these stages.

The target design spectrum depends on the seismic characteristics of the region and on local ground conditions [52]. International regulations differ in detail but follow similar methodologies. Design spectra typically have three regions: the constant spectral acceleration region (short period), the constant spectral velocity region (medium period), and the constant spectral displacement region (long period). The transitions between regions are set by corner periods.

A class for the design spectrum calculation was implemented. It takes the parameters required by the regulation as input and returns spectral accelerations and the corresponding periods as a two-dimensional array. The spectrum generation module exposes lower and upper period bounds as configuration, so the same class can be extended to other regulations. The TBEC function takes S_s (spectral acceleration at short period), S_1 (spectral acceleration at one second), and S_c (soil class) as input. A generic design spectrum is shown in Figure 1. The software implements the target spectrum formulation specified by the Turkish Building Earthquake Code 2018 [50]. The algorithm converts the mapped short-period (S_S) and one-second period (S_1) spectral accelerations into design spectral accelerations (S_{DS} and S_{D1}) using the local site coefficients (F_S and F_1) determined by the user-defined soil class:

$$\mathrm{S_{DS}} = S_s \times F_S \tag{1}$$

$$\mathrm{S_{D1}} = S_1 \times F_1 \tag{2}$$

Subsequently, the algorithm calculates the spectrum corner periods, T_A and T_B, which govern the constant acceleration regions of the response spectrum:

$$\mathrm{T_A} = 0.2(S_{D1}/S_{DS}) \tag{3}$$

$$\mathrm{T_B} = S_{D1}/S_{DS} \tag{4}$$

Using these parameters, the TBDYSpectrum module mathematically constructs the piecewise elastic design spectrum $S_{ae}(T)$ across the relevant period ranges.

The white noise signal is the basis of the generated ground motion. White noise is a random signal with equal intensity across frequencies and therefore a constant power spectral density. A perfect white noise signal cannot be produced in practice, but random number generators yield a close approximation. The software offers two methods for generating it.

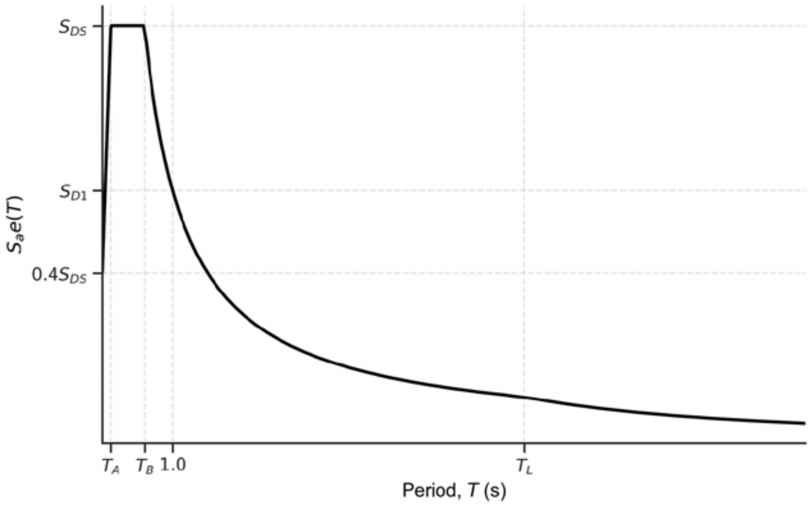

Figure 1. Generic elastic design response spectrum

The first method uses the standard pseudo-random number generator from modern computational libraries — specifically, NumPy's [53] built-in generator, based on the Mersenne Twister algorithm [54]. The generate_white_noise function samples from a normal distribution with user-specified mean and standard deviation. The time array is built with linear spacing:

$$t_i = i \cdot \Delta t, \quad i = 0,1,2, \dots, N-1 \tag{5}$$

where Δt is the time step and N is the total number of samples calculated as $N = [duration/\Delta t] + 1$. The acceleration values are generated using:

$$a_i \sim \mathcal{N}(\mu, \sigma^2) \tag{6}$$

where μ and σ represent the mean and standard deviation of the Gaussian distribution, respectively. This method provides excellent statistical properties and computational efficiency, making it suitable for most practical applications.

The second method uses a Linear Congruential Generator (LCG), exposed through the generate_linear_congruential_noise function. The LCG gives finer control over the generation process and is reproducible across computational platforms. The recurrence relation is:

$$x_{\{n+1\}} = (a \cdot x_n + c) \; mod \; m \tag{7}$$

where a is the multiplier, c is the increment, and m is the modulus. The default parameters used are $a = 1664525$, $c = 1013904223$, and $m = 2^{32}$, which are well-established values that provide good statistical properties [55]. The uniform random values generated by the LCG are then transformed to Gaussian distribution using the Box-Muller transformation:

$$z_1 = \sqrt{-2\backslash ln(u_1)} \times \cos(2\pi u_2) \tag{8}$$

$$z_2 = \sqrt{-2\backslash ln(u_1)} \times \sin(2\pi u_2) \tag{9}$$

where u_1 and u_2 are independent uniform random variables in the interval [0,1), and z_1, z_2 are independent standard normal random variables. The final noise signal is then scaled to achieve the desired statistical properties:

$$a(t_i) = \left(\frac{z_i - \bar{z}}{\sigma_z}\right)\sigma + \mu \tag{10}$$

where $\bar{z}$ and σ are the sample mean and standard deviation of the generated values, respectively. This normalization ensures that the output signal has exactly the specified mean (μ) and standard deviation (σ).

The raw white noise is far from the desired ground-motion characteristics, so a filter must be applied. Many filters could be used; the two most common are the Kanai–Tajimi filter [56,57] and the Clough-Penzien filter [58].

The Clough-Penzien filter is an extension of the Kanai-Tajimi filter that incorporates a high-pass filter component to remove unrealistic low-frequency content. This filter requires four parameters: ω_g (ground dominant angular frequency), ζ_g (ground damping ratio), ω_f (filter angular frequency), and ζ_f (filter damping ratio). In the standard implementation, ω_f and ζ_f are typically set to fixed values (e.g., $\omega_f = 0.1\ rad/s$ and $\zeta_f = 0.6$), while ω_g and ζ_g are user-specified parameters that control the dominant frequency content of the generated motion. In the optimization-based version of the software, all four parameters can be treated as optimization variables to achieve better spectral matching.

When filtering stage is completed, a low-pass filter is applied to remove high-frequency noise that may be present in the signal. A fourth-order Butterworth low-pass filter with a cutoff frequency corresponding to a period of $T_c = 0.025$ seconds (i.e., $f_c = 40\ Hz$) is used. This cutoff frequency value is selected to suppress high-frequency content beyond the engineering relevant range. Which is consistent and common in other studies [59-61]. This filtering step ensures that the generated ground motion does not contain unrealistic high-frequency components that could adversely affect structural response calculations.

After the initial filtering, the signal usually goes through enveloping and spectral matching to shape its temporal and spectral character. Here, an empirical scaling step is inserted before spectral matching to cut the number of iterations needed for convergence. A target Peak Ground Acceleration (PGA) is estimated from a formula tied to the Turkish Building Earthquake Code. The empirical PGA estimator is a function of the short-period spectral acceleration (S_s), the one-second spectral acceleration (S_1), and the site soil class, and reflects the code's intent across site conditions. The function selects coefficients by soil class so the resulting PGA stays consistent with the regulatory framework.

Alongside this code-specific estimator, the software bundles several ground motion prediction equations (GMPEs) for PGA: the Sabetta–Pugliese model [62], the Graizer-Kalkan model [63], and the Campbell-Bozorgnia model [64]. Each account for earthquake magnitude, source-to-site distance, site conditions (e.g., V_{s30}), and (where applicable) fault mechanism and focal depth. With several estimators available, users can pick the most appropriate one for their application or compare results across frameworks.

The choice of PGA estimator depends on the application and available information. For code-compliant design in Türkiye, the TBEC empirical estimator is the natural pick, since it is calibrated to the code's spectral parameters. For research applications, or when seismological source parameters (magnitude, distance, etc.) are known, the GMPE-based methods (Sabetta–Pugliese, Graizer–Kalkan, Campbell–Bozorgnia) tend to give more accurate estimates. Note that this PGA scaling phase is optional and serves primarily to provide a reasonable starting point for the spectral matching process, thereby reducing the number of iterations required for convergence.

After scaling, the enveloping phase is applied. Many enveloping approaches exist. This study uses the Saragoni–Hart envelope function [65] and a custom envelope function. Real ground motions show a gradual buildup of energy, a strong-motion phase, and a decay period; the software provides two envelope functions that reproduce this temporal shape.

The first approach uses the Saragoni–Hart envelope function, implemented through the create_saragoni_hart_envelope method:

$$I(t) = \alpha t^{\beta} e^{-\theta t} \tag{11}$$

where α, β, and θ are envelope parameters that control the shape and characteristics of the temporal modulation. The parameter α serves as a scaling factor, β controls the rate of initial amplitude growth, and θ governs the exponential decay rate. This formulation ensures that the envelope starts from zero, reaches a maximum value, and then decays exponentially, closely resembling the energy release pattern of natural earthquakes.

The second approach is a custom three-phase envelope function, exposed through the create_custom_envelope method. This piecewise function splits the ground motion duration into a rise phase, a steady phase, and a decay phase:

$$I(t) = \begin{cases} \left(\dfrac{t}{t_{rise}}\right)^2 & if\ 0 \le t \le t_{rise} \\ 1 & if\ t_{rise} < t \le t_{decaystart} \\ e^{-c(t-t_{decaystart})} & if\ t_{decaystart} < t \end{cases} \tag{12}$$

where $t_{rise} = r_{rise} \cdot T_{total}$, $t_{decay\_start} = t_{rise} + r_{steady} \cdot T_{total}$, r_{rise} and r_{steady} are the ratios of rise and steady durations to the total duration, respectively, c is the decay factor, and T_{total} is the total duration of the ground motion. This formulation gives independent control over the buildup, strong-motion, and decay phases.

In this study, spectral matching is used to close the discrepancy between the time-domain acceleration record’s response spectrum computed for single-degree-of-freedom systems with damping $\zeta = 0.05$ and the target design spectrum through an iterative procedure. The method relies on frequency-domain amplitude scaling and applies corrections at each iteration to reduce the mismatch.

First, the response spectrum of the uncorrected acceleration record $S_a^{cur}(T_i)$ is computed on the same period vector (T_i) as the target spectrum $S_a^{tar}(T_i)$. The correction ratio for each period is

$$r_i = \frac{S_a^{tar}(T_i)}{S_a^{cur}(T_i)}, \quad i = 1,2,\dots,N \tag{13}$$

Spectral matching requires careful tuning; therefore, the correction capability at each step is bounded. To ensure numerical stability and prevent over-correction, these ratios are clipped between lower and upper bounds:

$$r_i^{clip} = \min(r_{max}, \max(r_i, r_{min})) \tag{14}$$

In practice, $\mathrm{r}_{\mathrm{min}} = 5 \cdot 10^{-5}$ and $\mathrm{r}_{\mathrm{max}} = 15$ are used, although these values can be adjusted by the user. Since the matching is performed in the frequency domain, the period-based ratios are mapped to frequency via $\mathrm{f}_{\mathrm{i}} = 1/\mathrm{T}_{\mathrm{i}}$, and linear interpolation is applied to obtain a continuous correction function over frequency. The interpolant $\mathrm{r}^{\mathrm{int}}(f)$ is then sampled at the FFT frequency bins of the one-sided spectrum.

The Fast Fourier Transform of the current acceleration series $\mathcal{F}\{\mathrm{a(t)}\} = \mathrm{A(f)}$ is computed and amplitudes are scaled as

$$\tilde{A}(f) = r^{int}(f)A(f) \tag{15}$$

Applying the inverse FFT yields a candidate time series:

$$\tilde{a}(t) = \mathcal{F}^{-1}\{\tilde{A}(f)\} \tag{16}$$

At the end of each iteration, baseline correction is applied to $\tilde{a}(t)$ to remove low-frequency drift, and the updated $S_a^{cur}(T_i)$ is recomputed using SDOF response analysis.

Error measures are based on the relative differences between the target and current spectra. Evaluation is restricted to a frequency mask $\mathrm{f} \in [0.1,25]\ Hz$ (equivalently, a selected period range). The average and maximum errors are

$$\epsilon_{avg} = \frac{1}{N_\Omega}\sum_{i\in\Omega}\left|\frac{S_a^{cur}(T_i) - S_a^{tar}(T_i)}{S_a^{tar}(T_i)}\right|, \quad \epsilon_{max} = \max_{i\in\Omega}\left|\frac{S_a^{cur}(T_i) - S_a^{tar}(T_i)}{S_a^{tar}(T_i)}\right| \tag{17}$$

The iterative process terminates when $\epsilon_{avg} \leq 0.075$ and $\epsilon_{max} \leq 0.15$. A composite performance metric is also tracked at each step:

$$J = \omega_{avg}\epsilon_{avg} + \omega_{max}\epsilon_{max}, \quad \omega_{avg} = 0.95, \quad \omega_{max} = 0.05 \tag{18}$$

The iteration with the minimum metric is stored as the best solution, and the procedure stops early after two consecutive non-improving steps. This default value was selected after consecutive try-outs. Usually, algorithm achieves its best solutions in first 10 iteration. However, to show this divergence, algorithm’s maximum iteration and maximum non improved iteration values are set to 30 and 15 respectively in example section. All analyses use $\zeta = 0.05$. The usage of damping ratio as $\zeta = 0.05$ is common practice for both literature and regulations [50]. However, for specific cases, user can change this value also.

In addition to spectral matching phase, algorithm reports certain metrics to user when this process is completed. These features are, Significant Durations (D_{5-95} and D_{5-75}) Arias Intensity (I_a), Cumulative Absolute Velocity (CAV), Peak Ground Velocity (PGV), Peak Ground Displacement (PGD), PGV/PGA ratio, and signal nonstationarity characteristics including zero-crossing rate and time of peak ground acceleration (t_{PGA}). To ensure the physical accuracy of the integrated velocity and displacement time series, a second-order baseline correction is implemented by applying a high-pass Butterworth filter to remove low-frequency numerical integration drift. Because these parameters are calculated in the post-processing stage after the matching iterations are finalized, they do not introduce any computational overhead to the main optimization loop.

It should be noted that the software includes two versions: a standard version (agmg.py) and an optimization-based version (agmg_TLBO.py). In the optimization version, the spectral matching process is embedded within a Teaching-Learning-Based Optimization algorithm that optimizes seven parameters simultaneously: ω_g, ζ_g, ω_f, ζ_f, t_{rise_ratio}, t_{steady_ratio}, and c (decay factor). The parameter bounds for the TLBO optimization are: $\omega_g, \omega_f \in [0.1,15]\ rad/s, \zeta_g, \zeta_f \in [0.01,0.7]$, and $t_{rise\_ratio}, t_{steady\_ratio}, c \in [0,1]$. These parameters and their boundaries are presented in Table 1. The objective function for the TLBO optimization is defined as:

$$f_{obj} = 0.5 \cdot \epsilon_{avg} + 0.5\epsilon_{max} \tag{19}$$

For computational efficiency, the TLBO version uses more aggressive spectral matching settings with $max\_iterations = 10$ and $max\_no\_improvement = 2$ for each individual evaluation, as the optimization algorithm itself performs multiple evaluations.

Table 1. TLBO Parameter Bounds

Parameter	Lower Bound	Upper Bound
$\omega_g (rad/s)$	0.1	15
ζ_g	0.01	0.7
$\omega_f (rad/s)$	0.1	15
ζ_f	0.01	0.7
t_{rise_ratio}	0	1
t_{steady_ratio}	0	1
$c\ (decay\ ratio)$	0	1

The approach has two practical advantages for structural engineering work: smoothing corrections through frequency-domain interpolation mitigates localized oscillations along the period axis that would otherwise produce time-domain fluctuations, and bounding the ratios prevents over-amplification and numerical instability. Applying baseline correction at every iteration suppresses low-frequency drift and improves the consistency of the computed response spectra.

III. IMPLEMENTATION

The software is written in Python; the full source code can be found in an external repository [51]. Each module encapsulates one stage of the artificial ground motion (AGM) process: spectrum generation, initial motion synthesis, envelope shaping, spectral analysis, spectral matching, and output visualization. The modular split keeps the code maintainable and lets users substitute or customize individual components.

Figure 2, sketches the software's structure and the interactions between modules. Auxiliary functions outside the AGM workflow (data-formatting utilities, optional plotting) are omitted for clarity.

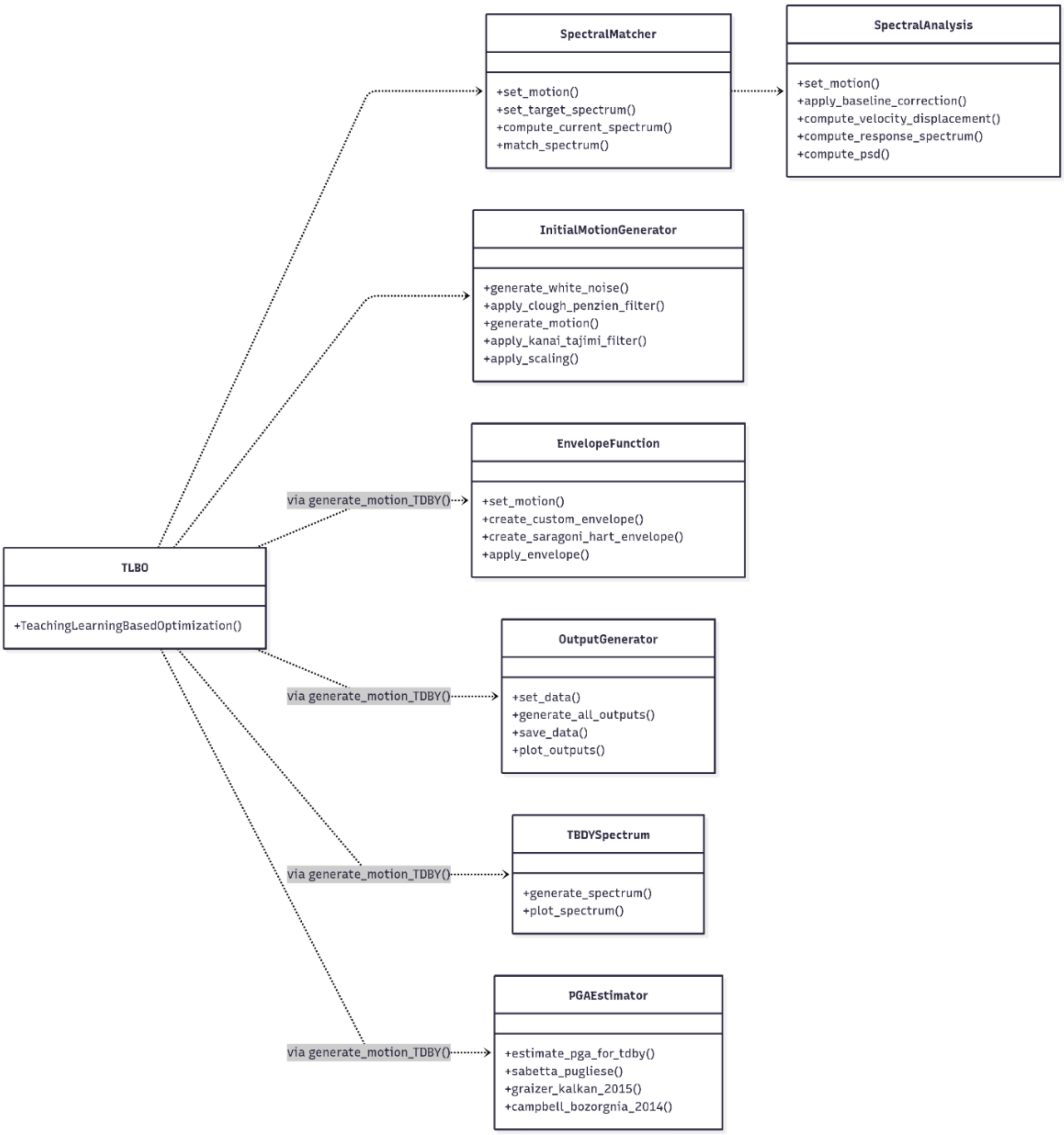

Figure 2. Object-oriented structure of the software

Algorithm 1 formalizes the core workflow, from input parameter specification to the generation and evaluation of the artificial ground motion record. It outlines the sequence of computational steps: spectrum calculation, initial motion generation, filtering, envelope application, baseline correction, response spectrum computation, and iterative spectral matching. Optional steps for visualization and reporting are also covered. Reporting functions can output JSON, CSV, or plain text. The modular design lets the software be adapted to different regulatory requirements, ground motion characteristics, or research objectives. An optimization-based version, based on the TLBO algorithm [66,67], is also included; it tunes seven parameters simultaneously, as noted earlier, to push spectral matching further. This version runs much longer because of the iterative optimization. It is named agmg_TLBO.py and is structured so users can change the optimization parameters, bounds, and objective function for specific needs.

Algorithm 1. generate motion TBEC workflow

```
1:   Inputs: Ss, S1, SoilClass∈{ZA,ZB,ZC,ZD,ZE}, max iterations, max non improvement, duration, Δt, pga
     ∈{tbdy, value}, ωg , ζg , name, imageoutput
2:   Create output directory: name outputs
     Compute target spectrum:
3:       TBDYSpectrum.generate spectrum(Ss,S1,SoilClass, min period=0.001,
         max period=8.0, num points=300, log scale=True)
4:   if pga == tbdy then
5:       pga ←PGAEstimator.estimate pga for tbdy(Ss,S1,SoilClass)
6:   Else
7:       pga ←float(pga )
8:   end if
     Generate Clough–Penzien motion:
9:       (t,a) ←InitialMotionGenerator.generate clough penzien motion(duration,Δt,ωg ,ζg,
         ωf =0.1,ζf =0.6,target pga=pga)
10:  Low-pass filter (Butterworth 4th):
         Tc=2.5 ×10−2 s, fc=1/Tc, apply filtfilt ⇒a←afiltered
11:  PSD (Welch): f, Pxx ←signal.welch(a, fs=1/Δt, nperseg=1024, scaling=density)
12:  Envelope: create custom with rrise=0.15, rsteady=0.05, c=0.8; apply to (t,a)
13:  Baseline correction: cutoff f=0.1 Hz; compute v(t) and u(t)
14:  Response spectrum: compute on periods with damping ζ=0.05
15:  Spectral matching setup: set (t,a) and target spectrum in SpectralMatcher
     Run match spectrum with:
16:      max iterations, tolerance avg=0.075, tolerance max=0.15, ζ=0.05, f ∈[0.1,25] Hz
         max ratio=15.0, min ratio=5 ×10−5
         wavg=0.95, wmax=0.05, max no improvement
17:  if imageoutput then
18:  Save target spectrum, filtered motion, PSD, envelope, spectra comparison, acceleration comparison,
     convergence figures
19:  Export report via OutputGenerator using matched records and parameters
20:  end if
21:  Returns: best average error, best maximum error
```

IV. AN EXAMPLE OF PROCESS

The complete case study presented in this section can be reproduced by any external user with a standard Python environment. After cloning the repository and installing the dependencies (numpy, scipy, matplotlib), the case study is regenerated with a single function call. Because the pseudo-random generator is seeded (seed = 3), the generated record, all reported time-domain metrics, and output figures can be reproduced. An illustrative example is generated using the agmg.py script. The parameters cover a typical seismic design scenario. The spectral acceleration at short period (S_s) and at one second (S_1) are set to 1.3 and 0.4, respectively, representing moderate-to-high seismicity. The soil class is ZB, a medium-dense profile that influences the shape and amplification of the target response spectrum. Maximum iterations for spectral matching are set to 30, with 15 consecutive non-improvement iterations allowed before early termination. The total duration is 40 seconds, with a time step (Δ_t) of 0.01 seconds. The peak ground acceleration follows the TBEC empirical approach (pga_ = "tbdy"). The parameters ω_g and ξ_g the natural frequency and damping ratio of the ground filter are set to 15.0 rad/s and 0.6 to capture the frequency content and energy dissipation of the motion. As shown in Algorithm 2, the output directory is named 'example', and graphical outputs are enabled. For reproducibility, the random seed is fixed via seed=3; Users can omit this parameter for stochastic variation.

Algorithm 2. Parameters of the generate_motion_TBDY Function

```
best_avg_error, best_max_error = generate_motion_TBDY(Ss=1.3, S1=0.4, soil_class='ZB',
max_iterations=30, max_non_improvement=15, duration=40, dt=0.01, pga_="TBDY", omega_g=15.0,
zeta_g=0.6, name='seeded', imageoutput=True, seed=3)
```

As mentioned in theoretical background, the first step is to generate target spectrum. After that, the initial motion is generated. The initial motion that generated with previously mentioned parameters can be seen in Figure 3a. To create the initial motion in this example, the empirically formulated PGA estimator and Clough-Penzien filter is used. When the initial motion is ready, the custom enveloping function is also applied to the motion. This enveloping function, differences between initial and enveloped motion is shown in Figure 3b.

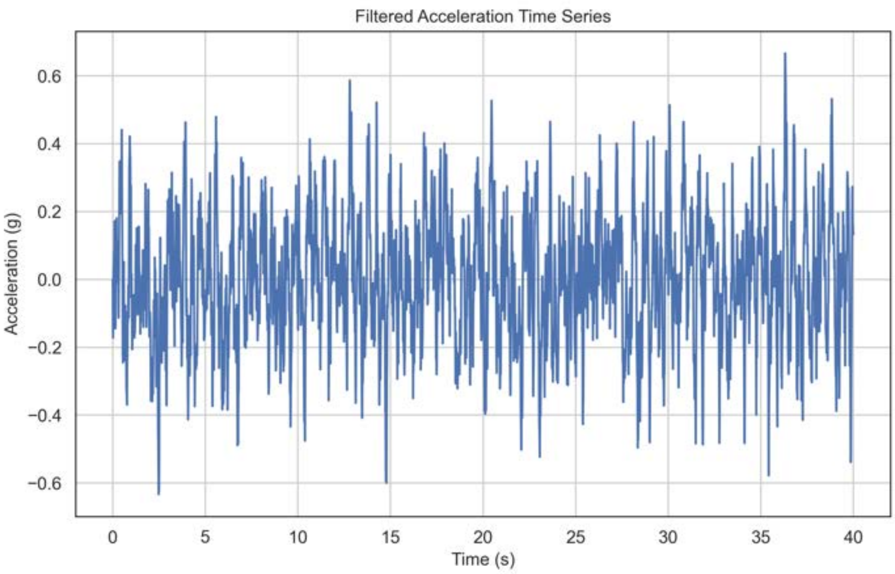

Figure 3a. The raw filtered (Clough–Penzien + Butterworth low-pass) acceleration time series before enveloping

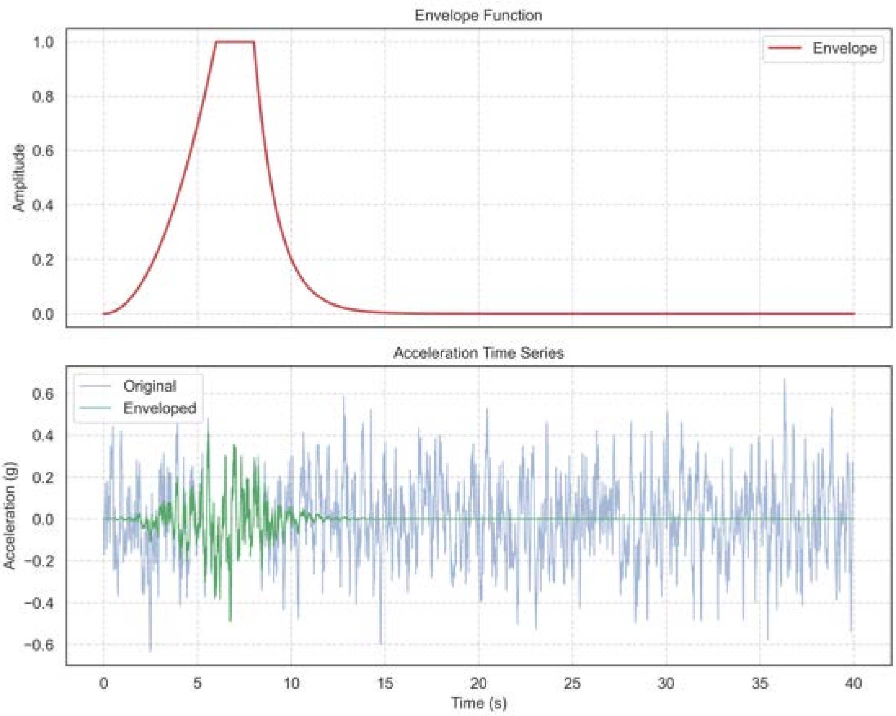

Figure 3b. The custom three-phase envelope function (top) and the resulting enveloped acceleration time series overlaid on the original (bottom)

Figure 3. Initial and enveloped motion generation

In this study, the algorithms that used for artificial ground motion generation showed acceptable compliance for mid and higher periods but lower value periods (higher frequencies) are extremely high. These excessive high-frequency components primarily originate from the inherent broadband nature of the initial white noise seed and the numerical artifacts introduced during the iterative frequency-domain amplitude scaling. To solve this problem, a low pass filter is applied. To show this process power spectral density and response spectrum of the motion is shown in Figure 4.

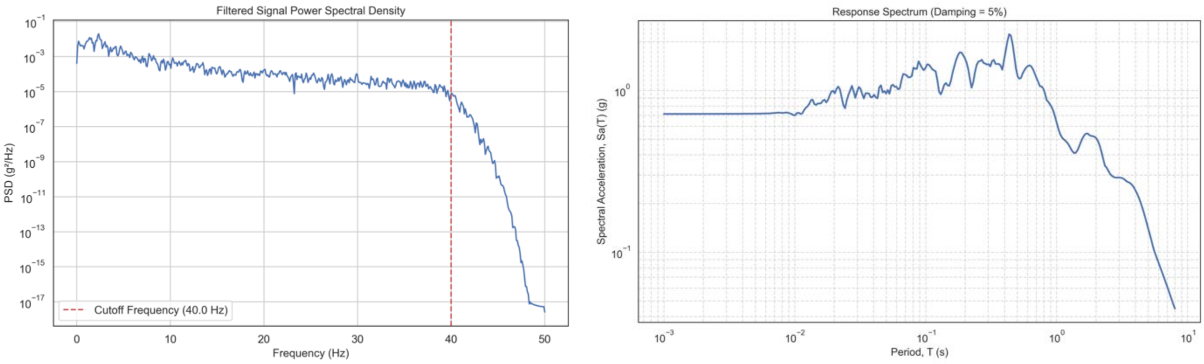

Figure 4. Spectral properties of the filtered signal: (left) power spectral density with the 40 Hz low-pass cutoff (dashed line) suppressing engineering-irrelevant high-frequency content; (right) the corresponding 5%-damped acceleration response spectrum of the initial motion before spectral matching

After the generation of initial ground motion, the response spectrum of the motion can be relatively compliant with the target spectrum. However, for engineering purposes, the motion should be more compliant with the target spectrum. To eliminate this difference as much as possible, spectral matching is applied. Theoretical background of the spectral matching process is explained in the previous section. It has been observed that the spectral matching process usually converges to target spectrum for a few iterations. After the maximum convergence, also usually the spectral matching drifts from its aim. To prevent this situation maximum iteration and maximum non improvement iteration parameters are added. But in this example, to show this situation, maximum non improvement iteration is set to 15 and maximum iteration is set to 30. The convergence process is shown in Figure 5. As can be seen in the figure, the average difference is acceptable, but the maximum difference is above the acceptable limit. These limit values are pre-defined by the user and can be changed for the purpose or the restrictions of the specific case. But as mentioned before, there is an optimization version of the spectral matching process function to tune specific parameters to achieve significant improvements. However, this function is very time consuming. Thus, for practical purposes, this usage is not demonstrated in this study. Note that, for most cases, the non-improvement iteration parameter can be set between 3 and 5 and maximum iteration parameter can be set between 10 and 20. The final version of the motion and spectrogram can be seen in Figure 6. The response spectrum of the motion after the spectral matching process can be seen in Figure 7. Other calculated metrics for this example are, Significant Durations (D_{5-95} and D_{5-75}) of 5.24 s and 3.89 s, Arias Intensity (I_a) of 1.013 m/s, Cumulative Absolute Velocity (CAV) of 5.789 m/s, Peak Ground Velocity (PGV) of 0.3049 m/s, Peak Ground Displacement (PGD) of 0.126 m, and a PGV/PGA ratio of 0.096 s. These values are consistent with stiff-soil records of comparable peak acceleration (PGA ≈ 0.3 g) from shallow crustal events along the North Anatolian Fault Zone (e.g., the 1999 Kocaeli/Düzce earthquakes), for which PGV is typically in the order of 25–45 cm/s and the PGV/PGA ratio clusters around 0.10 s these values are both in line with the generated record (PGV = 30.5

cm/s, PGV/PGA = 0.096 s) [68]. The zero-crossing rate is reported as 8.38 Hz with the peak acceleration occurring at 7.34 s. These values are highly reasonable and seismologically consistent for a design earthquake on a stiff soil profile (ZB) with a peak ground acceleration of 0.324 g. Specifically, the PGV and PGD values are well within the typical range for such strong motions, confirming that the second-order baseline correction effectively eliminates numerical integration drift without distorting the physical characteristics of the generated ground motion.

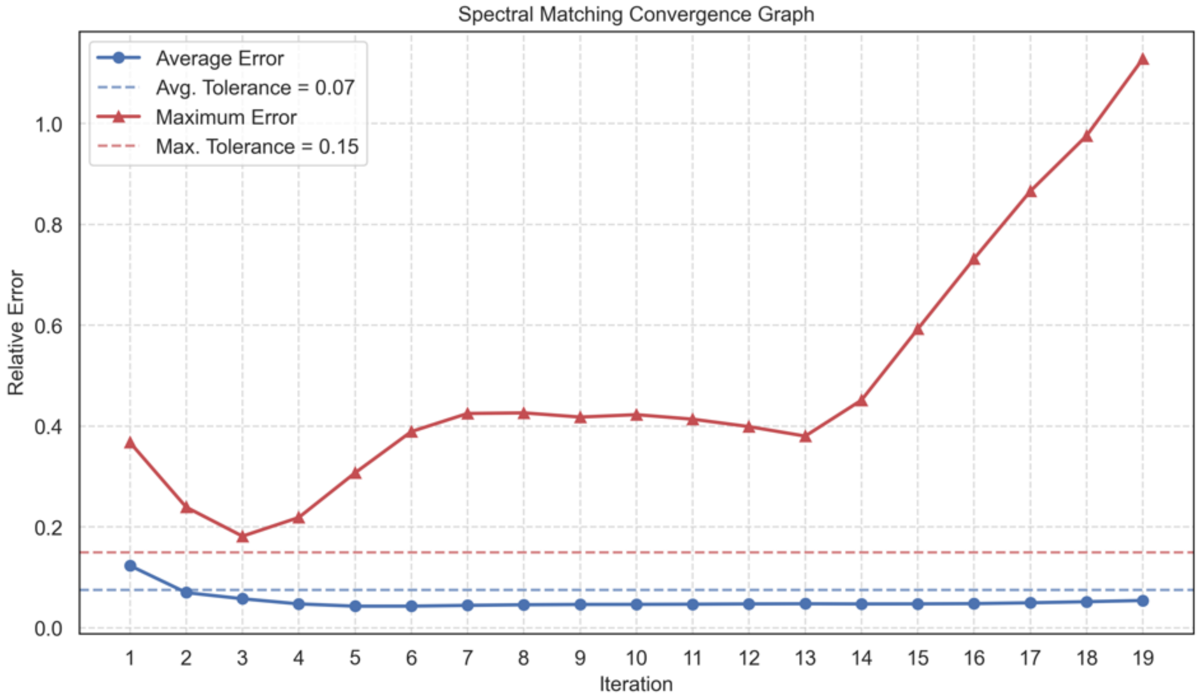

Figure 5. Convergence of the spectral matching

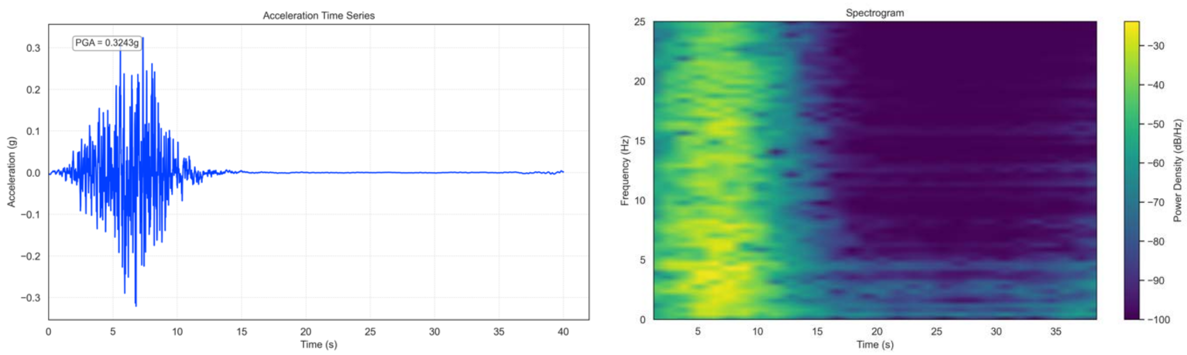

Figure 6. Final matched motion: (left) the spectrally matched acceleration time series (PGA = 0.324 g) and (right) time–frequency spectrogram, illustrating the non-stationary energy distribution imposed by the envelope

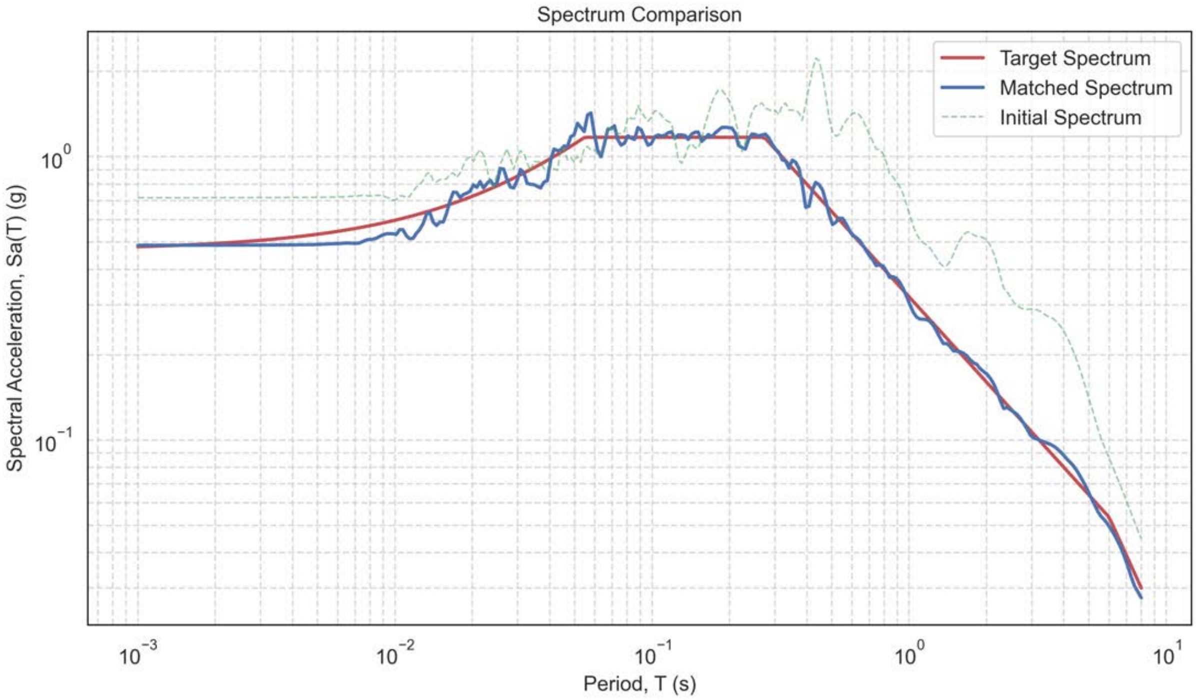

Figure 7. Comparison of the 5%-damped response spectra

V. PARAMETRIC ROBUSTNESS ANALYSIS

In this section, the robustness of the proposed algorithm is evaluated by systematically varying key input parameters: S_s, S_1, and S_c. These parameters are fundamental in defining the target response spectrum and, consequently, the characteristics of the generated ground motion. A parametric study was run across combinations of these three inputs, generating 2,500 artificial ground motion records. For each combination, the algorithm was executed five times to account for randomness in the pseudo-random generation. Operational parameters such as maximum iterations and non-improvement limits were held tight to test the algorithm under restrictive conditions.

The primary evaluation metric is the average relative difference between the target design spectrum and the final spectrum after matching. The 2,500-record analysis returns a stable result: the mean average spectral matching error across the database is 4.94%, and 99.52% of records fall below the 10% engineering threshold.

Figure 8 summarizes the distribution; most error values cluster around 5%, and only 12 simulations (0.48%) exceed the 10% limit. Figure 8a shows that lower S_s values carry slightly higher average errors and greater variability. These outliers concentrate at extreme low-amplitude regional hazard levels. There, dividing by very small target spectral values inflates the relative error mathematically, even though the absolute spectral differences are negligible for engineering purposes. A similar pattern of increased relative variability appears for higher S_1 values in Figure 8b.

For site conditions, an analysis of variance returns consistent performance across all profiles. Only minor variations appear between stiff rock (ZA) and soft soil (ZE) classes, and the matching results remain within acceptable limits. The default software settings hold up across the tested parameter ranges and produce code-compliant ground motions.

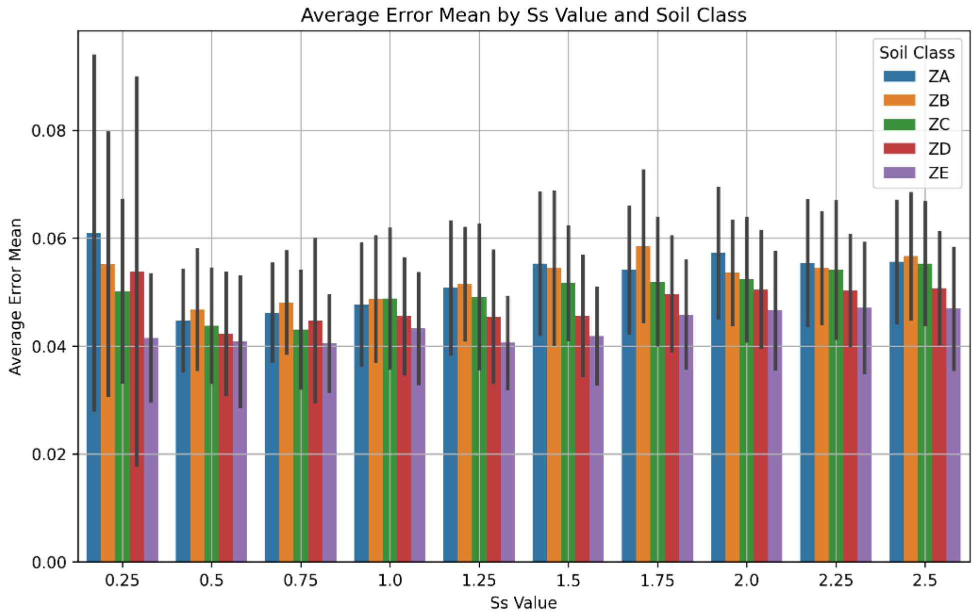

Figure 8a. Average error by Ss value and soil class

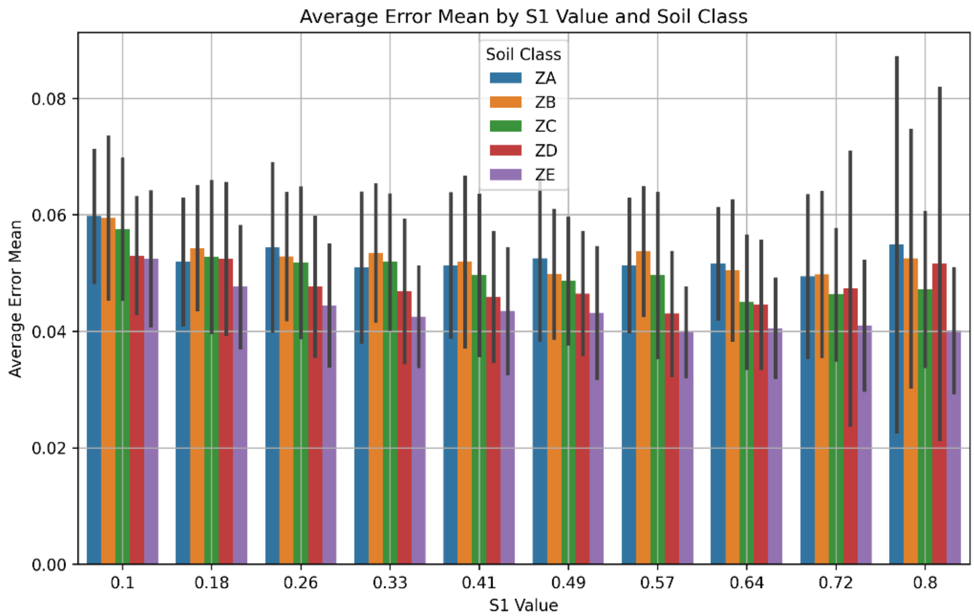

Figure 9b. Average error by S1 value and soil class

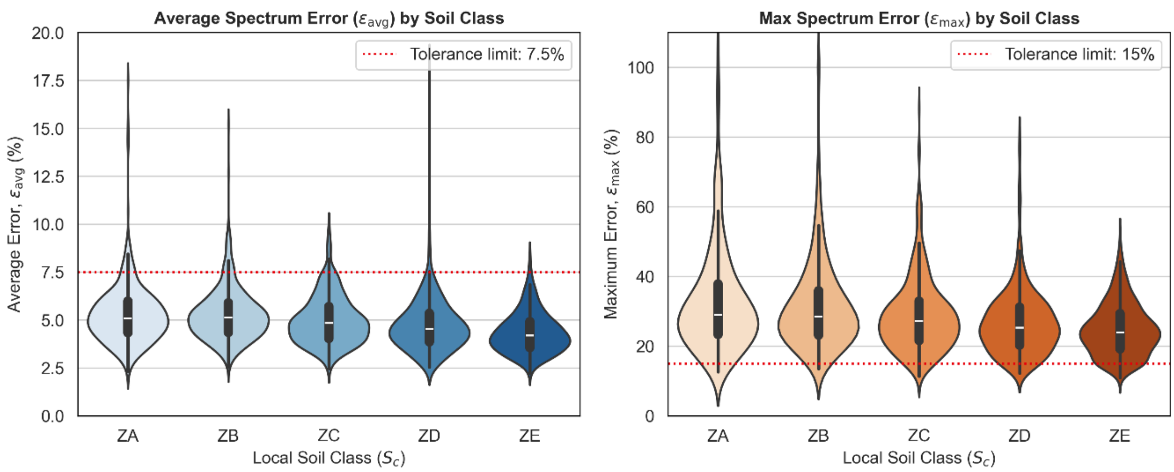

Figure 10c. Error by soil class

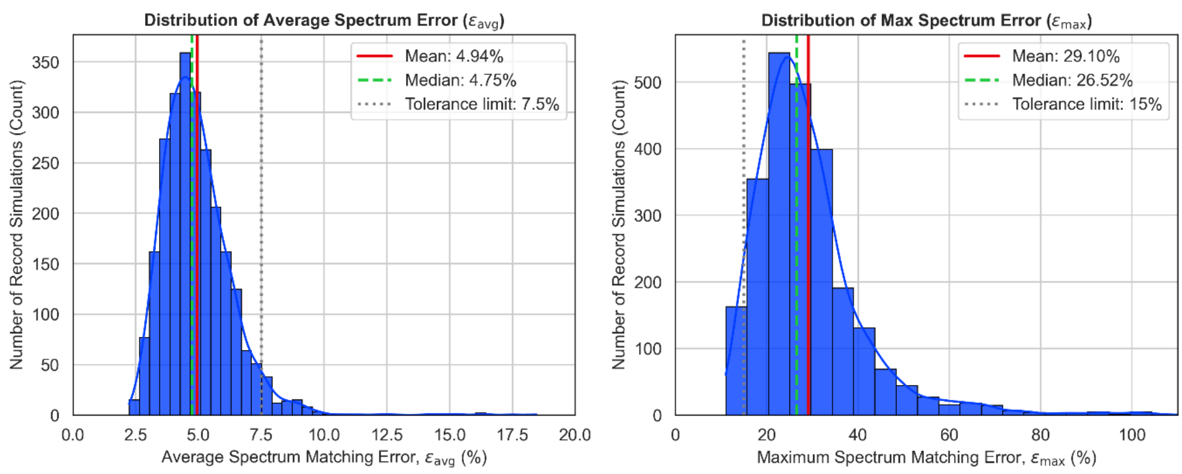

Figure 11d. Global error distribution

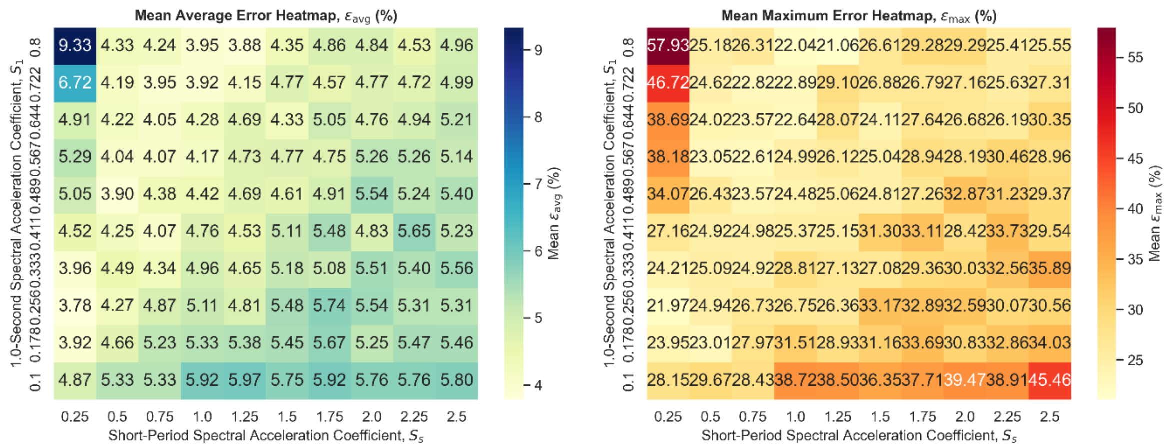

Figure 12e. Sensitivity heatmap

Figure 13. Error analysis

VI. DISCUSSION

This study presents an open-source Python software for generating artificial ground motions that match a target response spectrum for time-domain seismic analysis. Synthetic motions are needed when international ground motion databases are insufficient, or when specific engineering objectives must be met. The software handles the process through a set of bounded but independent modules. The modular split makes the code maintenance for further studies and lets users generate spectra compliant with regulations including the Turkish Building Earthquake Code (TBEC 2018), and to plug in different algorithms.

In the proposed artificial ground motion generation framework, several internal algorithmic parameters (filter frequencies, envelope ratios, and spectral correction boundaries) are utilized. Rather than treating these as variables for optimization in the standard execution, they are assigned default values grounded in established structural dynamics and strong-motion seismology literature. For instance, the Clough-Penzien filter parameters ($\omega_f = 0.1\ rad/s$ and $\zeta_f = 0.6$) are adopted to effectively suppress the low-frequency singularity of the standard Kanai-Tajimi spectrum without distorting the core physical characteristics of the motion. Similarly, the baseline correction high-pass cutoff frequency of 0.1 Hz is selected to remove numerical integration drifts while preserving the engineering-relevant long-period content, consistent with standard strong-motion processing practices [69]. The spectral correction bounds ($r_{min} = 5 \times 10^{-5}$ and $r_{max} = 15$) were established via preliminary numerical trials to strike a balance between rapid amplitude scaling convergence and the prevention of high-frequency numerical instabilities. While the current scope of this study focuses on the robustness of the generation algorithm against design spectrum parameters, the modular nature of the open-source software inherently allows users to conduct custom sensitivity analyses on these internal algorithmic parameters tailored to specific seismological or engineering requirements.

Although the software is equipped with a robust post-processing module to calculate key time-domain and energy-based characteristics, such as significant durations (D_{5-95} and D_{5-75}), Arias intensity (I_a), Cumulative Absolute Velocity (CAV), Peak Ground Velocity (PGV), and Peak Ground Displacement (PGD), a notable limitation of the current implementation is that these parameters are not integrated as active calibration or optimization criteria within the spectral matching loop. The iterative convergence process relies exclusively on matching the target acceleration response spectrum. Consequently, while baseline correction ensures physically realistic and drift-free velocity and displacement profiles, the generated records may not automatically conform to specific empirical targets or ground motion prediction equations (GMPEs) for duration or energy content. Users are recommended to use the software's post-processing outputs as validation measures since non-spectral properties are important in nonlinear structural response and damage development. A suite of motions with different seeds and envelope parameters should be produced for applications that are extremely sensitive to energy dissipation and duration to choose records that meet the required time-domain characteristics and spectral compatibility.

While the proposed framework provides code-compliant ground motion generation process, several inherent limitations must be critically acknowledged. First, the algorithm relies fundamentally on spectrum-only matching. This frequency-domain scaling ensures high spectral compatibility but does not actively optimize phase characteristics or time-domain energy distribution. Consequently, the generated records demand careful validation before application in advanced nonlinear structural analyses, where duration and cyclic energy dissipation heavily dictate structural damage. Second, regarding region-specific ground motion characteristics, the default envelope functions are primarily calibrated for typical shallow crustal environments. Capturing unique regional wave propagation effects requires manual user tuning of the envelope parameters. Finally, the current formulation lacks the explicit generation of near-fault forward-directivity effects. The baseline algorithm generates broadband signals that do not inherently possess the distinct, coherent long-period velocity pulses characteristic of near-fault zones. For structures located within such proximity to active faults, users must rely on selecting appropriate initial seed motions with inherent pulse-like features prior to initiating the spectral matching process.

In tests conducted with various regulatory parameters, the spectra of the generated artificial ground motions converged to the target spectrum with an average error generally below 10%, and in more stringent test cases, this error was reduced to below 5%. To evaluate the adaptability of the algorithm under different soil conditions and spectral values, a comprehensive parametric robustness analysis was performed, generating a total of 2500 artificial ground motion records by systematically varying S_s, S_1, and Soil Class (S_c). The study also notes the existence of an optimization-based version of the algorithm employing the Teaching–Learning-Based Optimization (TLBO) method, which requires multiple trial runs for convergence but significantly increases computational time. Overall, the proposed software provides a reliable framework for generating spectrally compatible ground motions required in engineering applications. It should be noted that the parametric robustness analysis revealed relatively higher average errors at extreme low S_s and S_1 values. This divergence is not a physical limitation of the generated motions, but rather a mathematical artifact; dividing by infinitesimally small target spectral accelerations artificially inflates the relative error during computation, whereas the absolute spectral differences remain negligible for practical engineering applications.

VII. CONCLUSIONS

This study presents an open-source Python software for generating artificial ground motions compatible with target design spectra. The modular structure of the software allows extensions and adaptations. The generated ground motions have limitations and constraints in their scope and applicability. The findings can be listed as following:

- The algorithm generates motions which converge to target spectra with average errors generally lower than 10%. The findings reveal a convergence and reliability that is highly stable for common engineering design contexts.
- The software’s object-oriented architecture enables the use, modification, and customization of discrete stages of spectrum generation, filtering, enveloping and spectral matching in isolation.
- The methodology utilizes a frequency-domain spectral matching approach to ensure high regulatory compatibility. While highly efficient, this spectrum-only scaling preserves the phase characteristics of the initial motion rather than actively optimizing the time-domain energy distribution.
- Optimization-based method that uses TLBO algorithm is provided. This approach results better spectral convergence at the cost of higher computational effort.
- The internal filtering and temporal envelope hyperparameters directly govern the intensity and frequency characteristics of the generated ground motion. The default settings ensure stable convergence for standard regulatory scenarios. However, capturing complex near-fault effects requires a tailored approach. These internal parameters must be explicitly calibrated for such specific cases.

REFERENCES

1. Harmsen SC (2001) Mean and modal ε in the deaggregation of probabilistic ground motion. Bull Seismol Soc Am 91:1537–1552. https://doi.org/10.1785/0120000289
2. Chowdhury IN, Cabas A, Kaklamanos J, Kottke A, Gregor N (2024) Implications of input ground-motion selection techniques on site response analyses for different tectonic settings. Earthq Spectra 40:1521–1551. https://doi.org/10.1177/87552930241230917
3. McCallen D, Petrone F, Miah M, Pitarka A, Rodgers A, Abrahamson N (2021) EQSIM—A multidisciplinary framework for fault-to-structure earthquake simulations on exascale computers, part II: Regional simulations of building response. Earthq Spectra 37:736–761. https://doi.org/10.1177/8755293020970980
4. Rezaeian S, Powers PM, Altekruse J, Ahdi SK, Petersen MD, Shumway AM, Frankel AD, Wirth EA, Smith JA, Moschetti MP, Withers KB, Herrick JA (2024) The 2023 US National Seismic Hazard Model: Subduction ground-motion models. Earthq Spectra 40:1739–1786. https://doi.org/10.1177/87552930241243069
5. Goulet CA, Kishida T, Ancheta TD, Cramer CH, Darragh RB, Silva WJ, Hashash YM, Harmon J, Parker GA, Stewart JP, Youngs RR (2021) PEER NGA-East database. Earthq Spectra 37:1331–1353. https://doi.org/10.1177/87552930211015695
6. Atkinson GM (2005) Ground motions for earthquakes in southwestern British Columbia and northwestern Washington: Crustal, in-slab, and offshore events. Bull Seismol Soc Am 95:1027–1044. https://doi.org/10.1785/0120040182

7. Atkinson GM, Boore DM (2008) Erratum to empirical ground-motion relations for subduction zone earthquakes and their application to Cascadia and other regions. Bull Seismol Soc Am 98:2567–2569. https://doi.org/10.1785/0120080108
8. Yenier E, Atkinson GM (2015) Regionally adjustable generic ground-motion prediction equation based on equivalent point-source simulations: Application to central and eastern North America. Bull Seismol Soc Am 105:1989–2009. https://doi.org/10.1785/0120140332
9. Tayfur B (2025) Optimized model updating and site-specific seismic assessment of a historical masonry bridge. Structures 81:110190. https://doi.org/10.1016/j.istruc.2025.110190
10. Tayfur B, Tunca O, Artar M, Çarbaş S (2026) The effect of existing damage on the seismic performance of a historical masonry structure: A site-specific assessment. Bull Earthq Eng. https://doi.org/10.1007/s10518-026-02506-9
11. McCallen D, Pitarka A, Tang H, Nakata R, Mosalam KM, Petrone F, Günay S, Perez C (2025) An open-access simulated earthquake ground-motion database for an M7 Hayward Fault earthquake in the San Francisco Bay Region. Earthq Spectra 41:2560–2597. https://doi.org/10.1177/87552930251340960
12. Gregor N, Silva W, Wong I, Youngs R (2002) Ground-motion attenuation relationships for Cascadia subduction zone megathrust earthquakes based on a stochastic finite-fault model. Bull Seismol Soc Am 92:1923–1932. https://doi.org/10.1785/0120000260
13. Del Gaudio S, Hok S, Festa G, Causse M, Lancieri M (2018) Near-fault broadband ground motion simulations using empirical Green's functions: Application to the Upper Rhine Graben (France–Germany) case study. In: Dalguer LA, Fukushima Y, Irikura K, Wu C (eds) Best practices in physics-based fault rupture models for seismic hazard assessment of nuclear installations. Springer, Cham, pp 155–177. https://doi.org/10.1007/978-3-319-72709-7_10
14. Lavoué F, Froment B, Gélis C, Boué P, Chaljub E, Stehly L, Beauprêtre S, De Martin F, Gisselbrecht L, Pilz M, Moiriat D, Cushing EM (2025) Potential and limitations of noise-based surface-wave tomography for numerical site effect estimation: A case study in the French Rhône valley. C R Géosci 356:59–84. https://doi.org/10.5802/crgeos.243
15. McCallen D, Tang H, Wu S, Eckert E, Huang J, Petersson NA (2022) Coupling of regional geophysics and local soil-structure models in the EQSIM fault-to-structure earthquake simulation framework. Int J High Perform Comput Appl 36:78–92. https://doi.org/10.1177/10943420211019118
16. Parker GA, Baltay AS, Rekoske J, Thompson EM (2020) Repeatable source, path, and site effects from the 2019 M 7.1 Ridgecrest earthquake sequence. Bull Seismol Soc Am 110:1530–1548. https://doi.org/10.1785/0120200008
17. Miksat J, Wen KL, Wenzel F, Sokolov V, Chen CT (2010) Numerical modelling of ground motion in the Taipei Basin: Basin and source effects. Geophys J Int 183:1633–1647. https://doi.org/10.1111/j.1365-246x.2010.04818.x
18. Graizer V, Kalkan E (2007) Ground motion attenuation model for peak horizontal acceleration from shallow crustal earthquakes. Earthq Spectra 23:585–613. https://doi.org/10.1193/1.2755949
19. Islam MM, Persaud P, Thant M, Win K, Sandvol E (2025) Estimating site amplification variability in Yangon, Myanmar, from a dense nodal seismic array. Earthq Spectra 41:3168–3189. https://doi.org/10.1177/87552930251352843
20. Stewart JP, Parker GA, Atkinson GM, Boore DM, Hashash YMA, Silva WJ (2020) Ergodic site amplification model for central and eastern North America. Earthq Spectra 36:42–68. https://doi.org/10.1177/8755293019878185
21. Boyd OS, Churchwell D, Moschetti MP, Thompson EM, Chapman MC, Ilhan O, Pratt TL, Ahdi SK, Rezaeian S (2024) Sediment thickness map of United States Atlantic and Gulf Coastal Plain strata, and their influence on earthquake ground motions. Earthq Spectra 40:89–112. https://doi.org/10.1177/87552930231204880
22. Kohrangi M, Bazzurro P, Vamvatsikos D, Spillatura A (2017) Conditional spectrum-based ground motion record selection using average spectral acceleration. Earthq Eng Struct Dyn 46:1667–1685. https://doi.org/10.1002/eqe.2876
23. Dabaghi M, Der Kiureghian A (2017) Stochastic model for simulation of near-fault ground motions. Earthq Eng Struct Dyn 46:963–984. https://doi.org/10.1002/eqe.2839
24. Hashash YMA, Abrahamson NA, Olson SM, Hague S, Kim B (2015) Conditional mean spectra in site-specific seismic hazard evaluation for a major river crossing in the central United States. Earthq Spectra 31:47–69. https://doi.org/10.1193/033113eqs085m
25. Boore DM (2003) Simulation of ground motion using the stochastic method. Pure Appl Geophys 160:635–676. https://doi.org/10.1007/pl00012553
26. Han SW, Jee HW (2020) A numerical model for simulating ground motions for the Korean Peninsula. Appl Sci 10:1254. https://doi.org/10.3390/app10041254

27. Li J, Cheng F, Lin G, Wu C (2023) Improved hybrid method for the generation of ground motions compatible with the multi-damping design spectra. J Earthq Eng 27:2034–2060. https://doi.org/10.1080/13632469.2022.2095059
28. Atkinson GM (2000) Stochastic modeling of California ground motions. Bull Seismol Soc Am 90:255–274. https://doi.org/10.1785/0119990064
29. Rezaeian S, Der Kiureghian A (2008) A stochastic ground motion model with separable temporal and spectral nonstationarities. Earthq Eng Struct Dyn 37:1565–1584. https://doi.org/10.1002/eqe.831
30. Rezaeian S, Der Kiureghian A (2010) Simulation of synthetic ground motions for specified earthquake and site characteristics. Earthq Eng Struct Dyn 39:1155–1180. https://doi.org/10.1002/eqe.997
31. Rezaeian S, Der Kiureghian A (2012) Simulation of orthogonal horizontal ground motion components for specified earthquake and site characteristics. Earthq Eng Struct Dyn 41:335–353. https://doi.org/10.1002/eqe.1132
32. Komatitsch D, Liu Q, Tromp J, Süss P, Stidham C, Shaw JH (2004) Simulations of ground motion in the Los Angeles Basin based upon the spectral-element method. Bull Seismol Soc Am 94:187–206. https://doi.org/10.1785/0120030077
33. Paolucci R, Mazzieri I, Smerzini C (2015) Anatomy of strong ground motion: near-source records and three-dimensional physics-based numerical simulations of the Mw 6.0 2012 May 29 Po Plain earthquake, Italy. Geophys J Int 203:2001–2020. https://doi.org/10.1093/gji/ggv405
34. Viens L, Laurendeau A, Bonilla LF, Shapiro NM (2014) Broad-band acceleration time histories synthesis by coupling low-frequency ambient seismic field and high-frequency stochastic modelling. Geophys J Int 199:1784–1797. https://doi.org/10.1093/gji/ggu362
35. Evangelista L, del Gaudio S, Smerzini C, d'Onofrio A, Festa G, Iervolino I, Landolfi L, Paolucci R, Santo A, Silvestri F (2017) Physics-based seismic input for engineering applications: A case study in the Aterno river valley, central Italy. Bull Earthq Eng 15:2645–2671. https://doi.org/10.1007/s10518-017-0089-7
36. Jayalakshmi S, Dhanya J, Raghukanth STG, Mai PM (2021) Hybrid broadband ground motion simulations in the Indo-Gangetic basin for great Himalayan earthquake scenarios. Bull Earthq Eng 19:3319–3348. https://doi.org/10.1007/s10518-021-01094-0
37. Aquib TA, Mai PM (2024) Broadband ground-motion simulations with machine-learning-based high-frequency waves from Fourier neural operators. Bull Seismol Soc Am 114:2846–2868. https://doi.org/10.1785/0120240027
38. Palgunadi KH, Bergmeister A, Bosisio A, Ermert LA, Koroni M, Perraudin N, Dirmeier S, Meier MA (2025) High resolution seismic waveform generation using denoising diffusion. J Geophys Res Mach Learn Comput 2:e2025JH000862. https://doi.org/10.1029/2025JH000862
39. Avci-Karatas C (2022) Application of machine learning in prediction of shear capacity of headed steel studs in steel–concrete composite structures. Int J Steel Struct 22:539–556. https://doi.org/10.1007/s13296-022-00589-z
40. Avci-Karatas C (2022) Artificial neural network (ANN) based prediction of ultimate axial load capacity of concrete-filled steel tube columns (CFSTCs). Int J Steel Struct 22:1341–1358. https://doi.org/10.1007/s13296-022-00645-8
41. Avci-Karatas C, Celik OC, Ozmen Eruslu S (2019) Modeling of buckling restrained braces (BRBs) using full-scale experimental data. KSCE J Civ Eng 23:4431–4444. https://doi.org/10.1007/s12205-019-2430-y
42. Alamdari AS, Dabiri R, Jani R, Sarand FB (2021) Seismic zoning of Tabriz area by stochastic finite fault model considering site-specific soil effects. Soils Rocks 44:1–13. https://doi.org/10.28927/sr.2021.047220
43. Mazzieri I, Stupazzini M, Guidotti R, Smerzini C (2013) SPEED: SPectral elements in elastodynamics with discontinuous Galerkin: A non-conforming approach for 3D multi-scale problems. Int J Numer Methods Eng 95:991–1010. https://doi.org/10.1002/nme.4532
44. Paolucci R, Smerzini C, Vanini M (2021) BB-SPEEDset: A validated dataset of broadband near-source earthquake ground motions from 3D physics-based numerical simulations. Bull Seismol Soc Am 111:2527–2545. https://doi.org/10.1785/0120210089
45. Cacciola P (2010) A stochastic approach for generating spectrum compatible fully nonstationary earthquakes. Comput Struct 88:889–901. https://doi.org/10.1016/j.compstruc.2010.04.009
46. Boudina A, Hammoutene M (2021) Generation of seismic excitations compatible with target spectrum: Application to Eurocode 8. World J Eng 18:122–135. https://doi.org/10.1108/wje-02-2020-0042
47. Loviknes K, Kotha SR, Cotton F, Schorlemmer D (2021) Testing nonlinear amplification factors of ground-motion models. Bull Seismol Soc Am 111:2121–2137. https://doi.org/10.1785/0120200386
48. Kohrangi M, Vamvatsikos D, Bazzurro P (2017) Site dependence and record selection schemes for building fragility and regional loss assessment. Earthq Eng Struct Dyn 46:1625–1643. https://doi.org/10.1002/eqe.2873
49. Tao D, Lin J, Lu Z (2019) Time-frequency energy distribution of ground motion and its effect on the dynamic response of nonlinear structures. Sustainability 11:702. https://doi.org/10.3390/su11030702

50. Disaster and Emergency Management Authority (2018) Turkish Building Earthquake Code. AFAD, Ankara, Türkiye.
51. Tayfur B (2026) Artificial ground motion generation, v0.1.2. GitHub. https://github.com/btayfur/artificial-ground-motion. Accessed 23 May 2026
52. AFAD (2023) Türkiye Seismic Hazard Risk Map. Disaster and Emergency Management Authority. https://tdth.afad.gov.tr/. Accessed 25 May 2023
53. Harris CR, Millman KJ, van der Walt SJ, Gommers R, Virtanen P, Cournapeau D, Wieser E, Taylor J, Berg S, Smith NJ, Kern R, Picus M, Hoyer S, van Kerkwijk MH, Brett M, Haldane A, del Río JF, Wiebe M, Peterson P, Gérard-Marchant P, Sheppard K, Reddy T, Weckesser W, Abbasi H, Gohlke C, Oliphant TE (2020) Array programming with NumPy. Nature 585:357–362. https://doi.org/10.1038/s41586-020-2649-2
54. Matsumoto M, Nishimura T (1998) Mersenne twister: a 623-dimensionally equidistributed uniform pseudo-random number generator. ACM Trans Model Comput Simul 8:3–30. https://doi.org/10.1145/272991.272995
55. Knuth DE (1997) The art of computer programming, vol 2: seminumerical algorithms, 3rd edn. Addison-Wesley, Boston.
56. Kanai K (1957) Semi-empirical formula for the seismic characteristics of ground (structure). Trans Archit Inst Jpn 57.1:281–284. https://doi.org/10.3130/aijsaxx.57.1.0_281
57. Tajimi H (1960) A statistical method of determining the maximum response of a building structure during an earthquake. 2nd World Conference on Earthquake Engineering, Tokyo, Japan, Jul. 11–18, pp 781–797.
58. Clough RW, Penzien J (1995) Dynamics of structures, 3rd edn. Computers & Structures Inc, Berkeley.
59. Wei B, Yan L, Jiang L, Hu Z, Li S (2021) Errors of structural seismic responses caused by frequency filtering based on seismic wave synthesis. Soil Dyn Earthq Eng 149:106862. https://doi.org/10.1016/j.soildyn.2021.106862
60. Douglas J, Boore DM (2011) High-frequency filtering of strong-motion records. Bull Earthq Eng 9:395–409. https://doi.org/10.1007/s10518-010-9208-4
61. Lutes LD, Lilhanand K (1979) Frequency content in earthquake simulation. J Eng Mech Div 105:143–158. https://doi.org/10.1061/JMCEA3.0002448
62. Sabetta F, Pugliese A (1996) Estimation of response spectra and simulation of nonstationary earthquake ground motions. Bull Seismol Soc Am 86:337–352. https://doi.org/10.1785/bssa0860020337
63. Graizer V, Kalkan E (2015) Update of the Graizer-Kalkan ground-motion prediction equations for shallow crustal continental earthquakes. US Geological Survey Open-File Report 2015-1009, Reston, VA, USA. https://doi.org/10.3133/ofr20151009
64. Campbell KW, Bozorgnia Y (2014) NGA-West2 ground motion model for the average horizontal components of PGA, PGV, and 5% damped linear acceleration response spectra. Earthq Spectra 30:1087–1115. https://doi.org/10.1193/062913EQS175M
65. Saragoni GR, Hart GC (1973) Simulation of artificial earthquakes. Earthq Eng Struct Dyn 2:249–267. https://doi.org/10.1002/eqe.4290020305
66. Rao RV, Savsani VJ, Vakharia DP (2011) Teaching–learning-based optimization: A novel method for constrained mechanical design optimization problems. Comput Aided Des 43:303–315. https://doi.org/10.1016/j.cad.2010.12.015
67. Tayfur B, Kamiloğlu HA (2024) Optimization of cantilever retaining wall design using improved teaching-learning-based optimization algorithms. Firat Univ J Exp Comput Eng 3:134–150. https://doi.org/10.62520/fujece.1430236
68. AFAD (2023) Türkiye acceleration database and analysis system. Disaster and Emergency Management Authority. https://tadas.afad.gov.tr/list-event. Accessed 25 May 2023
69. Boore DM (2005) On pads and filters: Processing strong-motion data. Bull Seismol Soc Am 95:745–750. https://doi.org/10.1785/0120040160